Efficacy of Lincomycin HCl Loaded Chitosan Nanoparticles Gel for In-Vivo Wound Therapy in Female Rats Model: Revolutionizing Tissue-Regeneration and Cutaneous Applications

Rabia Zaheer , Aisha Sethi * , Khawar Abbas , Mudassar Mazher , Rida Saddique , Tahreem Arshad , Zunaira Choudary , Ali Ahsan , Amina Ishaq

Posted Date: 28 February 2025

doi: 10.20944/preprints202502.2311.v1

Keywords: Carbapol 940 gel; Lincomycin HCl; Invivo; Acute Toxicity Studies

 doi:10.20944/preprints202502.2311.v1

Article

Efficacy of Lincomycin HCl Loaded Chitosan Nanoparticles Gel for *In-Vivo* Wound Therapy in Female Rats Model: Revolutionizing Tissue-Regeneration and Cutaneous Applications

Rabia Zaheer [1], Aisha Sethi [1,*], Muhammad Khawar Abbas [2], Mudassar Mazher [3], Rida Saddique [4], Tahreem Arshad [5], Zunaira Choudary [4], Ali Ahsan [1] and Amina Ishaq [1]

[1] Department of Pharmaceutics. Faculty of Pharmaceutical Sciences. Government College University, Faisalabad. Pakistan. 38000
[2] Department of Physics. Government College University. Faisalabad. 38000. Pakistan
[3] College of Pharmacy. University of Gujrat. Pakistan.
[4] Department of Pharmacology. Faculty of Pharmaceutical Sciences. Government College University, Faisalabad. Pakistan. 38000
[5] Department of Pharmaceutics, Faculty of Pharmacy, The Islamia University Bahawalpur, Punjab, 63100. Pakistan.
* Correspondence: Aisha Sethi (ayeshasethi786@gcuf.edu.pk)

Abstract: This study revolves around the design/optimization of nanoparticles containing Lincomycin HCl, utilizing chitosan as a polymer and sodium tripolyphosphate as a cross-linker. The ionotropic gelation method was employed for nanoparticle preparation. An optimized formulation was subjected to accelerated stability studies and evaluated through various parameters including particle size (103 ± 43 nm), zeta potential, scanning electron microscopy, and Fourier transform infrared spectroscopy, differential scanning calorimetry, Scanning Electron microscopy (SEM/TEM) and powdered X-ray diffraction. The entrapment efficiency of nanoparticles increased with rising drug concentration up to 0.2 g. FTIR and thermal studies analysis confirmed the absence of interactions between the drug and other components. X-ray diffraction analysis indicated the amorphous nature of Lincomycin HCl within the nanoparticles. Accelerated stability assessment demonstrated the integrity of the formulation. Moreover, Lincomycin HCl effectively prevented rat infections compared to control groups during a two-week study. The LD50 of Lincomycin HCl in rats surpassed 100 mg/kg, with acute toxicity analysis revealing no significant changes between untreated and Lincomycin HCl-treated rats. Histopathological examination indicated no damage to heart, liver, or kidney tissues. Thus, it is reasonable to assert that Lincomycin HCl demonstrated substantial antimicrobial activity in rats, supporting its traditional medicinal usage.

Keywords: Carbapol 940 gel; Lincomycin HCl; *Invivo*; acute toxicity studies

1. Introduction

Drug delivery systems play a pivotal role in modern pharmaceuticals, aiming to safely and effectively transport therapeutic compounds within the body. These systems optimize drug release profiles, improving aspects such as absorption, distribution, and elimination, thereby enhancing product effectiveness, safety, patient compliance, and convenience. (Liu, Yang, Xiong, & Gu, 2016; Mandal et al., 2010). Various routes of administration, including non-invasive per-oral, trans-mucosal, topical, and intravenous, are employed to achieve precise targeting or manage systemic pharmacokinetics. (Mandal et al., 2010). However, challenges such as inadequate solubility, toxic side effects, and lack of precise targeting have necessitated the development of innovative drug delivery systems.

 doi:10.20944/preprints202502.2311.v1

Nanomedicine has emerged as a promising field, particularly in cancer therapy and immunodeficiency diseases, leveraging innovative drug delivery systems (NDDSs) to overcome the limitations of conventional formulations. (Jain, 2008). These NDDSs offer enhanced efficacy, stability, and bioavailability, addressing issues such as unpredictable release profiles and suboptimal drug delivery. This study aims to comprehensively examine SMART Nano carrier-based delivery systems and extended controlled-release drug delivery systems. These advanced systems sustain drug concentrations within the therapeutic window for prolonged periods, reducing administration frequency and improving patient compliance and therapeutic efficacy. Intravenous administration offers rapid and complete drug absorption but poses risks, particularly in critically ill patients. (Vikas, Arvind, Ashish, Gourav, & Vipasha, 2011). Alternative routes, such as topical delivery, present safer options, with transdermal drug delivery showing promise for systemic distribution.

Topical drug administration offers advantages such as improved patient compliance, sustained release, and reduced gastrointestinal disturbances. Topical drug delivery provides sustained action, improved absorption, and reduced fluctuations in drug levels. It is suitable for both localized and systemic treatment, offering convenience, painless administration, and self-medication options. However, its effects are slow and sustained, with the potential for skin irritation. Chitosan, a naturally occurring biopolymer, has garnered attention for its antimicrobial properties and biocompatibility (Mu, Chu, Liu, & Zhang, 2020). Chitosan nanoparticles (CSNPs) offer advantages such as enhanced antibacterial properties, controlled and sustained drug release, and improved solubility and stability. They serve as effective carriers for drugs, vaccines, and genes, with applications in wound healing and drug delivery systems. Advancements in drug delivery systems, particularly chitosan-based nanoparticles, hold promise for enhanced drug delivery and wound healing. These innovative systems offer improved efficacy, stability, and patient compliance, addressing the limitations of conventional formulations. Further research in this field is warranted to explore their full potential in clinical settings (Divya & Jisha, 2018).

2. Materials and Methods

2.1. Materials

Lincomycin HCl (gift sample from Majestic Pharma), Low molecular weight chitosan powder (biological extract, $(C_6H_{11}NO_4)$ n) was obtained from Sigma Aldrich, Acetic acid anhydride were obtained from the Government College University Faisalabad, Polyethylene glycol 400 (PEG 400) was purchased from sigma Aldrich, Sodium tripolyphosphate (STPP) was purchased from local store i.e. Idrees scientific store, Carbopol 940 (Sigma Aldrich), Distilled water and ethanol were obtained from majestic pharmaceuticals, Female Rats (provided by the Department of Pharmaceutical Sciences, GCUF). All the chemicals used were of Analytical grade.

2.2. Synthesis of Gel

Carbopol 940 was chosen as the gelling agent in this formulation. A 1% aqueous solution of Carbopol 940 was prepared and subjected to continuous stirring at 800 rpm for 1 hour using a magnetic stirrer. The pH of the solution was adjusted to a range of 6.2–6.8 by incorporating 0.05% triethanolamine. The gel was stacked with lincomycin HCl nanoparticles (LNPs) (Athavale et al., 2022) by adding dried nanoparticles comparable to 1% w/w lincomycin content. In the meantime, constant blending was kept up with. Carbopol was chosen for effective application because of its non-disturbing and non-harmful nature, soundness across a wide temperature reach, and nonappearance of excessive touchiness responses. (Noreen et al., 2021).

2.3. Preparation of Calibration Curve

Given its water-solvent nature, the adjustment bend for lincomycin was laid out in water. A stock arrangement (10 µg/mL) for the alignment bend and all referenced media was ready in water. To set up the essential stock arrangement, 100 mg of unadulterated medication was broken down in 100 mL of Milli-Q water, bringing about a centralization of 1 mg/mL or 1000 µg/mL.

 doi:10.20944/preprints202502.2311.v1

Utilizing the equation *C1V1 = C2V2*,

Hence, 10 mL of the essential stock arrangement was taken and weakened up to 100 mL, bringing about an optional stock arrangement convergence of 10 µg/mL. Series dilutions were prepared from the secondary stock solution in 10 mL volumetric flasks using water as a diluent. Various dilutions ranging from 2 to 12 µg/mL were prepared in triplicates using the equation $C_1V_1 = C_2V_2$. The calculated amount of stock solution was withdrawn and diluted up to 10 mL in volumetric flasks with water for each concentration. Prepared dilutions were bath-sonicated for 2 minutes and then analyzed on a UV spectrophotometer to measure the absorbance of each dilution at 196 nm. The results were plotted in graphical form with mean absorbance on the y-axis and concentration on the x-axis. An R^2 value of 0.999 was determined using MS Excel. (Najim, 2017).

2.4. Characterization Tools for the Gel

2.4.1. Materials-Related to Characterization Techniques

XRD analysis was utilized to examine crystallographic properties and structural composition using a Rigaku MiniFlex X-ray Diffractometer, with data analyzed using Jade XRD analysis software (Roy, Nayak, Maddiboyina, & Nandi, 2022). Field emission scanning electron microscopy (FE-SEM) was used to inspect the surface morphology and shape of the mesoporous silica nanoparticles (MSNs). Before imaging, the samples were decorated with gold. FE-SEM images were captured at various amplifications. Particle size and zeta potential of nanosuspension diluted in distilled water were analyzed using dynamic light scattering (DLS) with a Malvern NanoZS90 instrument. (Sobhani, Samani, Montaseri, & Khezri, 2017). Rheological studies of selected formulations were conducted using a Brookfield viscometer at 50 rpm for 60 seconds with spindle no. 64. Viscosity measurements were performed in triplicates (n = 3) at a temperature of 25 ± 0.5 ºC to analyze the effect of viscosity on drug accommodation, mobility, leakage from nanoparticles, and release mechanism (Basha, AbouSamra, Awad, & Mansy, 2018). FTIR spectroscopy was employed to assess the deposited coating's functional groups and stoichiometric features using a Shimadzu 8400S spectrometer in transmission mode (Popescu-Pelin et al., 2018). Thermal analysis using DSC was conducted to study the response of various substances to temperature changes, including chitosan, tripolyphosphate (TPP), lincomycin HCl, blank nanoparticles, and drug-loaded nanoparticles, utilizing a Differential Scanning Calorimeter. (Yassin et al., 2023). TGA was employed to analyze weight loss with temperature variations, providing insights into thermal stability (Cheah et al., 2023). Stability studies of chitosan-based nanoparticles were conducted at room temperature and within a specified temperature range over 90 days, periodically assessing size, zeta potential, and drug content. (M. S. Alqahtani et al., 2021).

2.4.2. Entrapment Efficiency (EE %) and Loading of Drug (LC %)

The entrapment efficiency of freshly prepared nanoformulations was determined by centrifuging 1 mL of the formulation at 6000 rpm for 30 minutes using a Nano centrifuge machine. (Skwarczynski et al., 2022). Supernatants were assessed using a UV spectrophotometer, and entrapment efficiency was calculated using the formula:

$$Entrapment\ Efficiency\ (\%) = \frac{Total\ amount\ of\ drug - Unentrapped\ drug}{Total\ amount\ of\ drug} \times 100$$

2.5. Wound Healing Evaluation

An in vivo study on wound healing was conducted using adult male Wistar rats, adhering to ethical guidelines and institutional review board approval. The study involved acute oral toxicity assessment, determination of acute antimicrobial effects, and evaluation of wound healing using non-invasive methods (Weng et al., 2020).

2.6. Statistical Analysis

 doi:10.20944/preprints202502.2311.v1

Statistical analysis was performed on experimental data using one-way and two-way ANOVA with Tukey multiple comparisons and Bonferroni post-test, respectively, with significant results at $p < 0.05$ (GraphPad Prism 5 software). Results were presented as mean ± SEM (n = 5(Pawar, Tetteh, Debrah, & Boateng, 2019).

3. Results and Discussion

3.1. Generation of Calibration Curve

The wavelength of maximum absorption (λ_{max}) for lincomycin HCl was 192 nm. We utilized a calibration curve constructed from pure analytical-grade lincomycin hydrochloride monohydrate to quantify the lincomycin content in a 0.6 mg/mL lincomycin hydrochloride sample derived from raw lincomycin HCl. Our analysis revealed a lincomycin content of 0.629 mg/mL in the sample, representing 104.9 % of the labeled amount. The coefficient of assurance (R2) for the adjustment not entirely set in stone to be 0.9997 (Najim, 2017). Our discoveries intently line up with those detailed by Najim (2017), who accomplished a R2 worth of 0.999 in a comparable report (Najim, 2017).

Table 1. The absorbance of lincomycin HCl on UV spectrophotometer.

Concentration (µg/ml)	Absorbance (au)
1	0.0495
2	0.2244
3	0.3922
4	0.551
5	0.7224
6	0.877

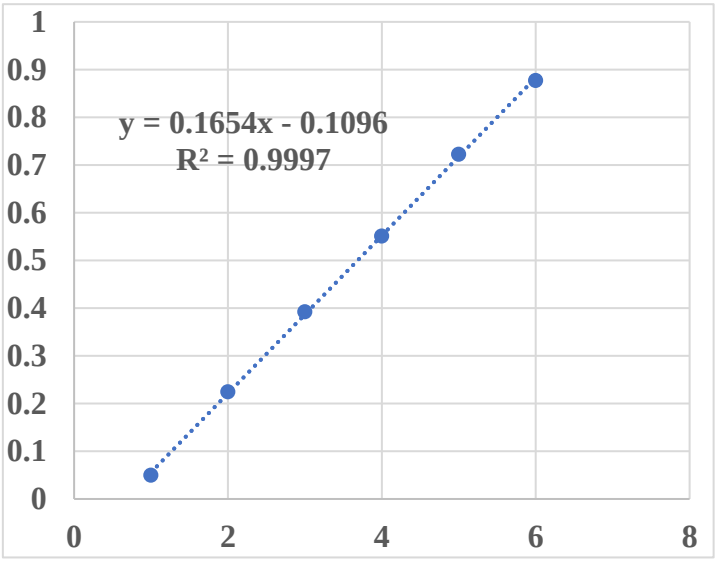

Figure 1. Calibration curve of lincomycin HCl.

3.2. Encapsulation Efficiency

The graphical portrayal of our information demonstrates that the medication showed greatest absorbance at a centralization of 4 µg/mL, recommending that this focus relates to the most noteworthy capture productivity (EE). This perception highlights the significance of advancing medication focus for accomplishing maximal EE in chitosan nanoparticles. Strangely, our discoveries adjust intimately with those detailed by Sobhani et al. (2017), where a comparative pattern was noticed: as the medication focus expanded, the ensnarement effectiveness likewise expanded, as well as the other way around (Sobhani et al., 2017). This parallelism in results further approves the

 doi:10.20944/preprints202502.2311.v1

meaning of our discoveries and builds up the thought that drug focus assumes a basic part in deciding the entanglement effectiveness of nanoparticles. These predictable patterns across concentrates on highlight the reproducibility and dependability of the noticed peculiarities, upgrading our trust in the ends drawn from our exploratory information. Such experiences are important for directing the levelheaded plan and detailing of medication stacked nanoparticles with streamlined entanglement proficiency, in this way boosting their restorative adequacy and likely clinical applications (Roy et al., 2022).

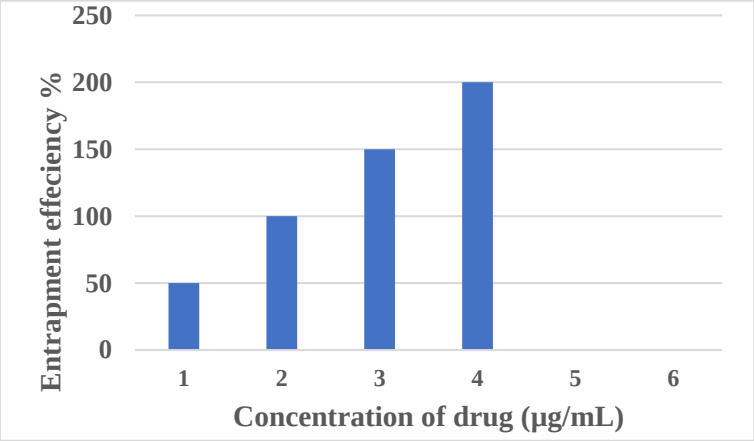

Figure 2. EE% of lincomycin HCl.

3.3. Particle Size and Zeta Potential

Molecule size PDI and zeta capability of lincomycin HCl stacked chitosan nanoparticles with various proportions of polymer and cross-linker separately

Table 2. Molecule size PDI and zeta capability of lincomycin HCl stacked chitosan nanoparticles with various proportions of polymer.

Formulation	Chitosan: STPP (mg)	Particle size (nm)	PDI	Zeta potential
F1	50:01	106.9	0.274	28 ± 4.91
F2	100:01	152.4	0.382	29.4 ± 4.91
F3	150:01	265	0.511	22.8 ± 5.54
F4	200:01	368.4	0.997	20 ± 46

Table 3. Particle size PDI and zeta potential of lincomycin HCl loaded chitosan nanoparticles with different ratios of cross-linker.

Formulations	Chitosan: STPP (mg)	particle size	PDI	zeta potential
F1	**3.2.1** **50:01**	106.9	0.274	24.7 ± 6.24
F2	50:02	125.4	0.232	22.9 ± 3.95
F3	50:03	113.2	0.465	22.6 ± 5.57
F4	50:04	103.2	0.243	20 ± 4.16

Table 2 gives an exhaustive outline of the effect of fluctuating convergences of chitosan to sodium tripolyphosphate (STPP) on the nano-definition. Our discoveries uncover an immediate connection between's how much chitosan used and the subsequent molecule size, with bigger molecule widths saw as chitosan focus increments while keeping the STPP fixation consistent. In particular, the mean molecule width shows a vertical pattern with diminishing polymer fixation. This pattern highlights the urgent job of chitosan in deciding the size of the nanoparticles, featuring its importance as a critical part in nanoparticle detailing. Strangely, our outcomes intently look like those detailed by Sobhani et al. (2017), where an ideal molecule breadth of 92 ± 112 nm was noticed (Sobhani et al., 2017). While our mean molecule breadth somewhat strays at 106 ± 82 nm, the likeness in

 doi:10.20944/preprints202502.2311.v1

patterns between the examinations highlights the consistency and reproducibility of the noticed peculiarities across various trial settings. This assembly in discoveries further approves the meaning of chitosan focus in affecting nanoparticle size and underlines the significance of streamlining detailing boundaries to accomplish wanted molecule attributes (Nguyen, Nguyen, Wang, Vo, and Nguyen, 2017).

Also, in one more table where the grouping of chitosan is held steady while changing the proportion of STPP, further bits of knowledge into the nanoparticle plan process are given. This trial configuration considers a more nuanced comprehension of what changes in the STPP fixation mean for molecule size, supplementing the discoveries got from fluctuating chitosan focuses. Together, these tables offer significant bits of knowledge into the complex interchange between definition boundaries and nanoparticle attributes, working with the reasonable plan and improvement of chitosan-based nanoformulations for different biomedical applications. Our perceptions, as nitty gritty in Table 3, highlight the basic job of STPP focus in balancing nanoparticle size. Remarkably, our discoveries uncover an unmistakable pattern wherein expanding the volume of STPP prompts a decrease in molecule size. The critical positive accuse related of chitosan, emerging from its serious level of deacetylation and protonation, manages chitosan atoms various potential cross-connecting destinations. At first, when the volume of STPP is under a specific limit, the response arrangement stays clear, showing an absence of noticeable opalescence. This clearness proposes that the STPP arrangement is deficient to work with the development of a cross-connected structure with chitosan. In any case, as the volume of STPP logically expands, there is a recognizable reduction in molecule size credited to the uplifted cross-connecting thickness among chitosan and STPP. Past a specific point, further expansions in the volume of STPP bring about the development of single, huge nanoparticles. This peculiarity happens as chitosan arrives at its greatest limit for cross-connecting, and the overabundance of STPP present decreases the surface charge thickness, compromising the solidness of these bigger particles during blending. This way, precariousness prompts the precipitation of these particles (F. Y. Alqahtani et al., 2019).

Amazingly, these perceptions adjust intimately with the discoveries of Sobhani et al. (2017), where a mean breadth of 45 ± 166 nm was accounted for. While our mean distance varies somewhat at 103 ± 97 nm, the all-encompassing pattern stays predictable. The arrangement of stable nanoparticles with improved steadiness and bioavailability highlights the meaning of enhancing STPP focus in chitosan-based nanoparticle details, working with their likely applications in different biomedical settings (Sobhani et al., 2017).

3.4. Impact of pH on Chitosan-Based NPs:

The effect of pH on chitosan-based nanoparticle size was explored by differing the pH inside the scope of 3.3 to 5.5. Our discoveries uncovered tremendous contrasts in nanoparticle conduct across various pH conditions. In plans described by basic chitosan to STPP mass proportion, modifications in pH brought about perceptible changes in suspension appearance. In particular, as the pH diminished under 5, the smooth white shade of the suspension lessened, demonstrating a disturbance in nanoparticle development. This peculiarity can be credited to the non-uniform molecule size conveyance saw at lower pH levels. Alternately, when the pH surpassed 5, the nanoparticle suspension showed up clear, recommending the presence of nanoparticles inside the plan. This perception highlights the pH-subordinate nature of chitosan, what capabilities as a frail electrolyte with a pKa worth of 6.5. The level of protonation of chitosan nanoparticles is complicatedly connected to the pH of the arrangement, impacting their soundness and conduct. Generally, our discoveries feature the basic job of pH in administering the arrangement and soundness of chitosan-based nanoparticles, highlighting the significance of pH enhancement in nanoparticle plan and improvement. (Container Jumah et al., 2020).

3.5. Effect of Stirring Speed on Particle Size and PDI

Table 4. Effect of stirring speed on particle size.

 doi:10.20944/preprints202502.2311.v1

Formulations	Chitosan: STPP	Stirring speed (rpm)	Particle size (nm)	PDI
U1	50:4	700	164 ± 57.14	0.627
U2	50:4	800	125 ± 64.78	0.232
U3	50:4	900	100.04 ± 79	0.275
U4	50:4	1000	97.25 ± 71	0.39

Our review inspected the effect of fluctuating blending speeds on the molecule size appropriation of nanoparticles. We saw that as the blending speed expanded from 700 rpm to 1100 rpm, there was a critical reduction in the molecule size circulation. This shows that higher blending speeds advance more effective scattering and blending of the parts, prompting more modest and more uniform nanoparticles. Notwithstanding, it is critical to take note of that past a specific point, further heightening of the mixing speed came about in a smaller top in the molecule size dissemination bend. Also, an aggregation of particles was seen around the 700 nm mark. This proposes that exorbitantly high mixing velocities might prompt agglomeration or grouping of particles, possibly affecting the homogeneity of the nanoparticle scattering. Generally speaking, our discoveries propose that legitimate fomentation, inside a specific scope of blending speeds, can upgrade the scattering of sodium tripolyphosphate (STPP) in the chitosan arrangement and increment shear powers, in this way working on the monodispersity of the nanoparticles. Notwithstanding, cautious improvement of blending boundaries is important to forestall unnecessary agglomeration and guarantee the consistency of the nanoparticle suspension (Algharib et al., 2022)

3.6. Impact of Chitosan (CS) Concentration on the Size of Nanoparticles (NPs)

In our examination, we investigated the effect of chitosan (CS) focus on the size of nanoparticles (NPs). As opposed to the relationship saw between zeta potential and antibacterial viability, we tracked down an immediate relationship between the convergence of chitosan and the size of the nanoparticles. This proposes that higher groupings of chitosan are corresponded with bigger nanoparticle sizes, while lower centralizations of chitosan lead to the development of more modest nanoparticles. (Ahmet, 2020).

3.7. Zeta Potential

Zeta potential is a basic figure deciding the solidness of suspensions in fluid arrangements, and it essentially impacts the antibacterial movement of chitosan nanoparticles (CS-NPs). Our examination plays divulged the vital part of zeta likely in molding the antibacterial viability of CS-NPs. In particular, we have found that higher zeta likely upsides of CS-NPs associate with additional articulated antibacterial impacts (Chandrasekaran et al., 2020). Prominently, our information show that the antibacterial movement of anti-microbial related CS-NPs is intently attached to their zeta potential. We noticed a decline in the zeta capability of chitosan-NPs upon the expansion of Lincomycin to shape half breed CS-NPs. This reduction in zeta potential might be ascribed to the positive charge gave by the STPP particles. Zeta potential estimations are regularly utilized to evaluate the connection of nanoparticles with charged particles or atoms. Our concentrate further highlights the meaning of zeta potential in accomplishing stable NP definitions. As portrayed in Table 2, plans F1 to F4 showed steadiness, with F1 meeting satisfactory models, displaying a polydispersity file (PDI) of 0.2 (Chandrasekaran, Kim, and Chun, 2020).

3.8. Field Emission Scanning Electron Microscopy (FE-SEM)

Using FE-SEM, the morphology and porous structure of the NPs were examined. The virtually monodispersed spherical shape of the NPs was revealed using FE-SEM micrographs. Furthermore, FE-SEM unequivocally demonstrated the presence of nanostructures and confirmed as shown in Figure 3.

 doi:10.20944/preprints202502.2311.v1

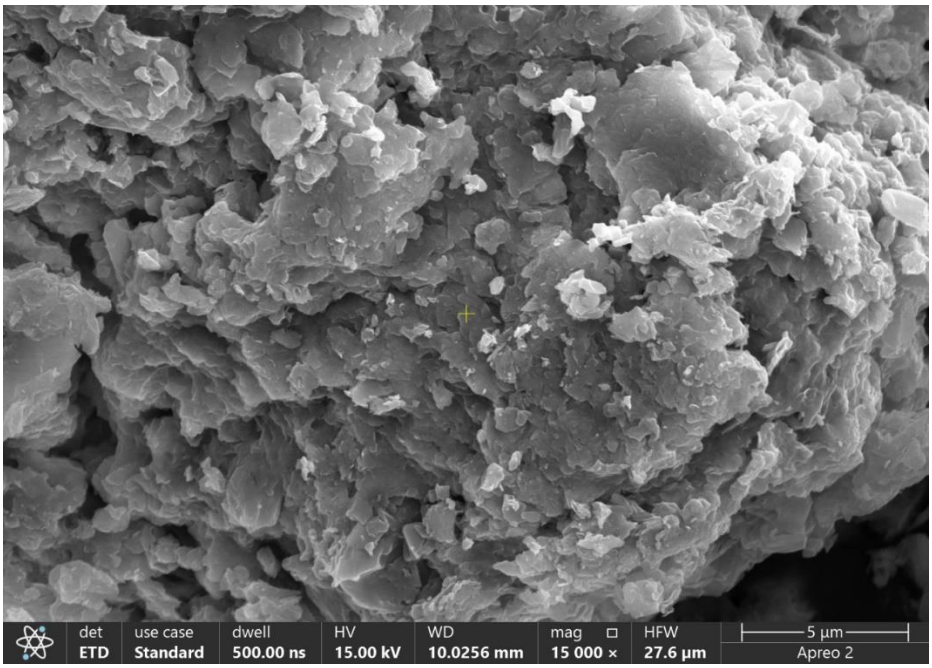

Figure 3. Field emission scanning electron microscopy of Lincomycin HCL loaded chitosan NPs gel.

3.9. Rheological Studies

The rheological properties, especially thickness, and pH, of the gel containing lincomycin-stacked chitosan nanoparticles are vital contemplations for grasping the definition's attributes and possible applications. (Saraiva et al., 2023). With a consistency worth of 240 Cp, the gel containing lincomycin-stacked chitosan nanoparticles shows a somewhat high thickness. Thickness is a key boundary that influences the stream conduct of liquids, and with regards to a gel, it impacts factors, for example, application ease, spread capacity, and steadiness. A consistency of 240 Cp shows a decently thick gel, which could offer good maintenance at the application site. This quality is invaluable for drug or clinical purposes where supported discharge and delayed contact with the objective region are wanted. On account of lincomycin-stacked chitosan nanoparticles, the high thickness might work with confined drug conveyance by supporting the adherence of the gel to explicit destinations, like injuries, empowering a controlled arrival of lincomycin over the long haul (Hejjaji, Smith, and Morris, 2018).

3.10. pH Range

The pH scope of 7.0 to 7.4 saw in the gel of chitosan nanoparticles and lincomycin-stacked chitosan nanoparticles falls inside the marginally fundamental to almost nonpartisan reach. pH is a basic calculate drug and clinical definitions, as it can influence drug steadiness, similarity, and expected disturbance to skin or tissues. Lincomycin, being pH-delicate, requires a climate helpful for its strength. pH goes from marginally fundamental to approach nonpartisan is for the most part good for keeping up with the steadiness of lincomycin. Outrageous pH values, either profoundly acidic or exceptionally basic, can prompt lincomycin debasement and lessen its adequacy. (Abd-Allah, Abdel-Aziz, and Nasr, 2020). Subsequently, the pH scope of 7.1 to 7.4 demonstrates that the definition is possible streamlined to save the steadiness of lincomycin inside the gel, fundamental for guaranteeing its adequacy upon application to the objective region, like skin or mucous layers. To put it plainly, the rheological properties, including consistency and pH, are vital elements in planning and assessing the appropriateness of lincomycin-stacked chitosan nanoparticles for drug or clinical use. The modestly high consistency might work with controlled drug delivery and maintenance, while the somewhat acidic to approach unbiased pH range upholds the dependability and adequacy of lincomycin inside the gel. These attributes all in all improve the definition's true capacity for confined drug conveyance and helpful viability. (Rajendran, Kumar, Houreld, and Abrahamse, 2018).

 doi:10.20944/preprints202502.2311.v1

This study's discoveries are steady with those of R. Kumar and Tyagi (2022), who revealed a pH esteem going from 6.99 to 7.01 for lincomycin gel.

3.11. Fourier Transform Infrared Spectroscopy

Fourier Transform Infrared Spectroscopy (FTIR) is a significant instrument for inspecting the cooperation among medications and polymers, revealing insight into bond developments, breakages, and practical gathering advances. The gave spectra portray the FTIR examinations of chitosan, lincomycin, sodium tripolyphosphate (STPP), chitosan/STPP nanoparticles, and chitosan/tripolyphosphate (TPP) based lincomycin nanoparticles. The FTIR range of chitosan uncovers a few conspicuous pinnacles demonstrative of its primary highlights. Outstandingly, the top at 468 cm-1 relates to the twisting vibration of the C-C ring skeleton, proposing the presence of chitin in chitosan. Other huge pinnacles incorporate those at 518.85 cm-1 (explicit chitosan vibrations), 584.43 cm-1 and 599.86 cm-1 (amide II and amide III vibrations), 839 cm-1 (glycosidic linkages), and a few others related with C-O, C-N, and C extending or twisting vibrations (Anicuta et al., 2010; Sethi et al., 2021; Tantala et al., 2019). Also, the FTIR range of lincomycin hydrochloride (HCl) gives experiences into its sub-atomic sythesis, but with less detectable pinnacles. Imperative pinnacles incorporate those around 468 cm-1 (possibly connected with C-H twisting), 518.85 cm-1 (C-H bowing), and 584.43 cm-1 (different sub-atomic vibrations), among others (R. Kumar and Tyagi, 2022; Ganjoo et al., 2016; He et al., 2016). The FTIR range of sodium tripolyphosphate (STPP) shows trademark tops related with phosphate gatherings and other utilitarian gatherings present in the particle. These incorporate tops at 433.98 cm-1, 474.49 cm-1, and 549.71 cm-1, relating to phosphate bunch vibrations, alongside others demonstrative of C-H, C-O, and P-O extending or bowing vibrations ((Gurses, Erkey, Kizilel, and Uzun, 2018; Wang et al., 2020; Yao et al., 2021). The FTIR spectra of chitosan/STPP nanoparticles and chitosan/TPP-based lincomycin nanoparticles display tops reflecting both chitosan and STPP/TPP, alongside likely commitments from lincomycin. These spectra show different vibrational modes related with chitosan, STPP/TPP, and lincomycin utilitarian gatherings, offering bits of knowledge into the creation and associations inside the nanoparticles ((Agarwal et al., 2018); (Grumezescu et al., 2019; Qing et al., 2021) In synopsis, FTIR examination gives point by point data about the atomic designs and cooperations inside the concentrated on frameworks, supporting the portrayal of chitosan-based nanoparticles and their medication stacked details.

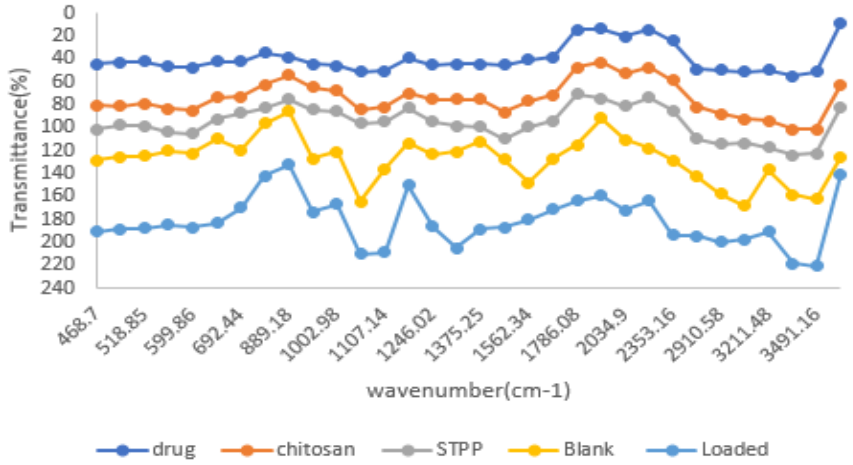

Figure 4. FTIR spectra of the drug, chitosan, STPP, blank and drug-loaded sample.

3.12. DSC (Differential Scanning Calorimetry)

DSC (Differential Scanning Calorimetry) examination was led on chitosan nanoparticles (NPs), lincomycin-stacked chitosan nanoparticles, lincomycin, STPP, and chitosan utilizing a TA Instruments USA model DSC2-OO4O7 series. This examination expected to screen any stage changes

 doi:10.20944/preprints202502.2311.v1

in the examples concerning both time and temperature under controlled conditions. The temperature (in °C) was plotted against the intensity stream (in W/g). The interaction included warming the heater from an underlying encompassing temperature, with a warming pace of 10 °C/min, up to a most extreme temperature of 300 °C. This warming was completed in a nitrogen environment with a stream pace of 10 mL/min-1. Such a strategy considers an intensive assessment of the warm properties of the NPs (Sethi et al., 2021). The warm attributes of lincomycin-stacked chitosan nanoparticles were investigated utilizing DSC-TGA thermograms. Assessment of lincomycin by DSC uncovered a minor top at 160 ºC followed by a sharp endothermic top at 165 ºC, as portrayed in Fig 4.19 (a). Then again, the thermogram of chitosan showed an endothermic top at 130 ºC. Initially, the DSC thermogram of low molecular weight chitosan nanoparticles (CSNPs) exhibited a sharp endothermic peak at 187.9 °C, as illustrated in fig 4.19 (b). This higher temperature indicated degradation concurrent with the breakdown of amine groups in low-molecular-weight chitosan nanoparticles at 200 °C. Incorporating lincomycin into chitosan nanoparticles revealed a minor endothermic peak at 110 ºC, followed by another peak at 120 ºC, and subsequently, an exothermic peak at 220°C. The abrupt changes in the peak after 200 ºC suggest that some reaction may have occurred at high temperatures leading to nanoparticle degradation (Fatima, Sheikh, Abourehab, & Kesharwani, 2022) The DSC thermogram of lincomycin-loaded CS-NPs exhibited a small curved endothermic peak at 130 °C, corresponding to the melting point of lincomycin (150 °C). This observation suggests that lincomycin was present in its crystalline form within the nanoparticles. Characterization of TGA thermograms was utilized to comprehend the modification pattern of the new polymer. Chemically cross-linked CS-NPs demonstrated higher thermal stability compared to non-cross-linked NPs. TGA analysis revealed mass losses at various temperatures, indicating disintegration and a reduction in the height and sharpness of endothermic peaks, primarily due to the improved thermal stability of cross-linked low molecular weight chitosan nanoparticles (CS-NPs)(Khalil et al., 2021). TGA thermograms indicated that CS-NPs (unloaded) exhibited decomposition temperatures nearly identical to those of lincomycin. After cross-linking with STPP, the endothermic peak of LMWCH shifted from 125.09 °C to 187 ºC, with TGA revealing a mass loss of 10.7%. These outcomes propose a substance communication among chitosan and STPP, as well as expanded inflexibility of the chitosan network at higher temperatures. The thermogravimetry bend demonstrated no adjustment of the liquefying reason behind lincomycin, connoting the shortfall of a synthetic communication among lincomycin and CS-NPs. These discoveries line up with comparative perceptions detailed in DSC-TGA thermograms for cross-connected nanoparticles, which displayed more prominent unbending nature and temperature security contrasted with non-cross-connected nanoparticles and moved endothermic tops to higher temperatures (Sethi, Ahmad, Huma, Khalid, and Ahmad, 2021).

 doi:10.20944/preprints202502.2311.v1

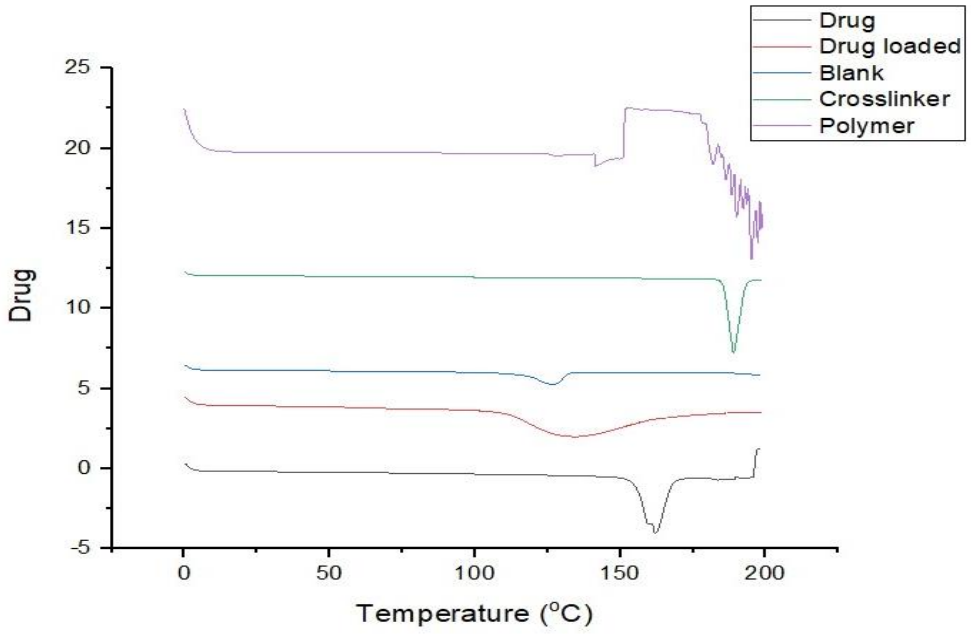

Figure 6. DSC analysis.

3.13. X-Ray Powder Diffraction (XRD) Analysis

The X-beam powder diffraction (XRD) examples of chitosan, chitosan nanoparticles, and lincomycin-stacked chitosan nanoparticles, portrayed in the figures, offer critical bits of knowledge into the primary attributes of these materials. These examples uncover particular elements revealing insight into their crystallinity and cross section constants (Khan, Yu, and Kim, 2020). Deciphering XRD information for a material like Lincomycin HCL includes dissecting pinnacles and powers to close its glasslike design and virtue. In the XRD example of chitosan, a noticeable diffraction top arises at a 2θ point of 19.99659°, showing a serious level of crystallinity inside the chitosan structure. The comparing precious stone grid constants (α) are determined to be 252, highlighting the coordinated, translucent nature of chitosan in its local structure (Marei, Abd El-Samie, Salah, Saad, and Elwahy, 2016). The presence of clear cut tops in the Lincomycin HCL XRD information recommends the example's somewhat unadulterated nature. The match between noticed tops and the normal Lincomycin HCL gem structure affirms the compound's presence. Notwithstanding, top expanding in certain areas of the XRD design shows that the example might contain more modest crystallites or underlying defects (Ahmad et al., 2019).

Conversely, the X-beam diffraction examples of chitosan nanoparticles and Lincomycin HCL-stacked chitosan nanoparticles display an eminent shortfall of pinnacles. This recommends that these nanoparticles miss the mark on same level of crystallinity as chitosan. Critically, the XRD profiles of chitosan nanoparticles and lincomycin-stacked nanoparticles are vague, suggesting that lincomycin stacking fundamentally affects the glasslike idea of chitosan. (Dish et al., 2020). These perceptions all in all help the end that the XRD example of chitosan is normal for an undefined polymer, while chitosan nanoparticles show a particular primary plan described by a more disarranged arrangement of polymer binds because of the crosslinking process.(Divya, Vijayan, George, and Jisha, 2017). In outline, the XRD information gives basic proof of the underlying contrasts among chitosan and its nanoparticles, featuring the shapeless idea of chitosan and the adjusted chain arrangement in the nanoparticles coming about because of the cross-connecting process. These discoveries have critical ramifications for understanding chitosan-based nanoparticles' properties and expected applications in different fields.

 doi:10.20944/preprints202502.2311.v1

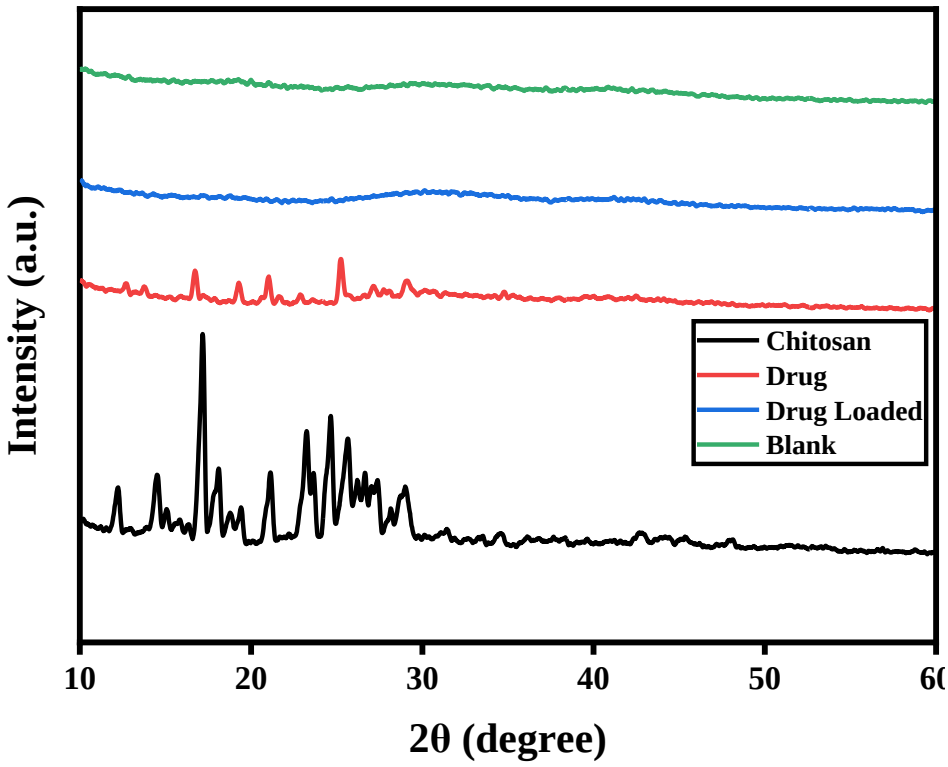

Figure 7. X-ray powder diffraction (XRD).

3.14. Stability Studies

These studies were directed to evaluate the colloidal dependability of chitosan-based nanoparticles created under ideal circumstances. The assessment was performed at room temperature and inside a temperature scope of 6 °C to 7 °C throughout different time stretches. Astoundingly, even following 20 days of capacity at room temperature, the suspension kept up with its visual lucidity with insignificant opalescence. Furthermore, there were no massive changes seen in molecule size or circulation during this term. These outcomes demonstrate that chitosan/STPP-based lincomycin nanoparticles display uncommon soundness under both room temperature and the somewhat cooler scope of 6 to 7 degrees Celsius (Gumustas et al., 2017). The steadiness noticed can be credited to a few elements, including a low ionic strength climate, reasonable pH conditions bringing about a last suspension pH of 5.8, high crosslinking thickness, little molecule size, slender molecule size dissemination, and great surface capability of the nanoparticles. Further improvement away soundness might actually be accomplished by bringing the capacity temperature down to 4ºC or integrating a cryoprotective specialist (Shantier, Elimam, Mohamed, and Gadkariem, 2017).

3.15. In Vivo Studies

Assessment of social adjustments and weight vacillations in rodents from control and lincomycin HCl treated bunches during intense poisonousness examination. In surveying intense harmfulness, a solitary oral portion of 100mg/kg fluid scattering was controlled. Eminently, no recognizable changes were identified in social or mental boundaries, and there were no announced occasions of mortality during the whole 14-day perception period, as nitty gritty in Table 5 This result firmly affirms the magnificent security profile of the plant. Such perceptions give vigorous proof supporting the case that the LD50 of lincomycin HCl surpasses 100mg/kg. The exhaustive assessment stresses the promising security parts of the given portion, supporting trust in the plant's low harmfulness potential (Noreen et al., 2021).

In the exhaustive assessment of intense harmfulness, a particular oral organization of a 100mg/kg watery scattering was used. Significantly, there were no way to see a modifications in conduct or mental boundaries, and no occasions of mortality were accounted for all through the

 doi:10.20944/preprints202502.2311.v1

whole 14-day perception period, as fastidiously kept in Table 6. Further examination of body weight uncovered a genuinely immaterial contrast between the benchmark group and the anti-infection treated bunch, as displayed in Table 6. These discoveries unequivocally support the statement that the LD50 of lincomycin HCl surpasses 100mg/kg. Such an exhaustive evaluation highlights the promising wellbeing qualities related with the controlled portion, supporting trust in the plant's strikingly low poisonousness potential. (Chhibber, Gondil, and Sinha, 2020)

Table 5. change in parameters in acute toxicity study.

Parameters	Observations of control and lincomycin HCl treated group														
	30 minutes			4 h			24 h			7 days			14 days		
	Control	Blank treated	L. HCL treated	Control	Blank treated	L. Hcl treated	Control	Blank treated	L.treated	Control	Blank treated	Ltreated	Control	Blank treated	L. treated
Eye colour	N	N	N	N	N	N	N	N	N	N	N	N	N	N	N
Pupil size	N	N	N	N	N	N	N	N	N	N	N	N	N	N	N
Salivation	N	N	N	N	N	N	N	N	N	N	N	N	N	N	N
Skin	N	N	N	N	N	N	N	N	N	N	N	N	N	N	N
Fur	N	N	N	N	N	N	N	N	N	N	N	N	N	N	N
Urine colour	N	N	N	N	N	N	N	N	N	N	N	N	N	N	N
Feces consistency	N	N	N	N	N	N	N	N	N	N	N	N	N	N	N
Convulsions & tremors	N	N	N	N	N	N	N	N	N	N	N	N	N	N	N
Itching	N	N	N	N	N	N	N	N	N	N	N	N	N	N	N
Coma	N	N	N	N	N	N	N	N	N	N	N	N	N	N	N
Sleep	N	N	N	N	N	N	N	N	N	N	N	N	N	N	N
Somatomotor activity &	N	N	N	N	N	N	N	N	N	N	N	N	N	N	N

 doi:10.20944/preprints202502.2311.v1

behavior pattern															

Table 6. (100mg/kg) on body weight (g) of rats in acute toxicity study.

Days	Control	Treatment (100mg/kg)
	Body weight (g)	
1	163.6±1.36	177.2±1.40 ^{ns}
7	171.2±1.98	174.2±0.86 ^{ns}
14	192.4±1.60	196.4±1.03 ^{ns}

3.16. Impact on Hematological and Biochemical Parameters in the Course of an Acute Toxicity Investigation

In the context of acute toxicity testing, a thorough examination of Complete Blood Count (CBC) was conducted, comparing the control group with the group treated with lincomycin HCl. The findings revealed no significant changes in most parameters, except for a notable variation in platelet count and white blood cell count, as delineated in Table 7 It's crucial to note that despite this variance, the platelet count remained within the normal range, reinforcing the conclusion that the tested lincomycin exhibits a favorable safety profile. An expansion in white platelet (WBC) count commonly shows actuation of the resistant framework because of contaminations brought about by Escherichia coli (E. coli) and Staphylococcus aureus (S. aureus). This disparity offers help for the attestation that the anti-infection has antimicrobial action, subsequently offering significant experiences into the general security evaluation (Chhibber et al., 2020).

Table 7. Effect of lincomycin NPs gel(100mg/kg) on hematological in acute toxicity study.

Parameters	Units	Normal Control	Treatment with a blank formulation	Treatment with loaded formulation
Haemoglobin	g/dl	11.4±0.298	12.78±0.306^{ns}	12.6±0.51^{ns}
TLC	$\times 10^9$/l	11.0±0.70	11.9±0.57 ^{ns}	12.0±0.55 ^{ns}
Total RBC	$\times 10^{12}$/l	4.20±0.19	6.54±0.16 ^{ns}	7.58±0.32 ^{ns}
HCT (PCV)	%	40.5±0.58	38.8±0.86 ^{ns}	40.6±0.68 ^{ns}
MCV	Fl	64.0±1.82	52.2±1.77 ^{ns}	53.6±1.34 ^{ns}
MCH	Pg	14.6±1.20	19.8±0.70 ^{ns}	16.6±0.65 ^{ns}
MCHC	%	35.6±0.65	35.2±1.00 ^{ns}	31.0±1.30 ^{ns}
Platelets	$\times 10^3$/uL	561.8±5.81	614.4±1.6***	971±2.0***
Neutrophils	%	36.9±2.44	44.8±1.29 ^{ns}	17±1.79 ^{ns}
Lymphocytes	%	23.8±1.65	39.6±1.22 ^{ns}	79±1.20 ^{ns}
Monocytes	%	2.74±0.73	3.2±0.81 ^{ns}	3.0±1.71 ^{ns}
Eosinophils	%	1.45±0.31	1.32±0.78	1.0±0.64
Total WBCs	10^3/uL	14.22±0.29	19.18±0.65	17±1.56

 doi:10.20944/preprints202502.2311.v1

Figure 7. The activity of wound healing.

During the underlying days, especially up to day 7, an eminent decrease in injury measurement is noticed, proposing a moderately quick mending process in the beginning phases. As time advances past day 7, the pace of decrease in injury breadth seems to decelerate, demonstrating a potential adjustment work in the injury recuperating process. Moving towards the later days, remarkably from day 10 to day 14, further decreases in injury widths are noted, demonstrating continuous recuperating and expected conclusion of the injuries (Pervaiz, Mushtaq, and Noreen, 2021). Despite the fact that there is some fluctuation in the information, particularly perceptible on day 7 and day 10, this could be ascribed to individual contrasts in the recuperating system or different elements affecting injury recuperation. Notwithstanding this changeability, the general pattern shows reliable injury mending, obvious from the diminishing width over the long run. By day 14, the injury measurements are essentially more modest, showing movement towards conclusion. It's important an unexpected diminishing in breadth for one of the injuries on day 14. This could be an exception or may require further examination to grasp the justification for such quick changes. Clinically, the information recommends good advancement in injury recuperating as displayed in Figure 8 (Pervaiz et al., 2021)

 doi:10.20944/preprints202502.2311.v1

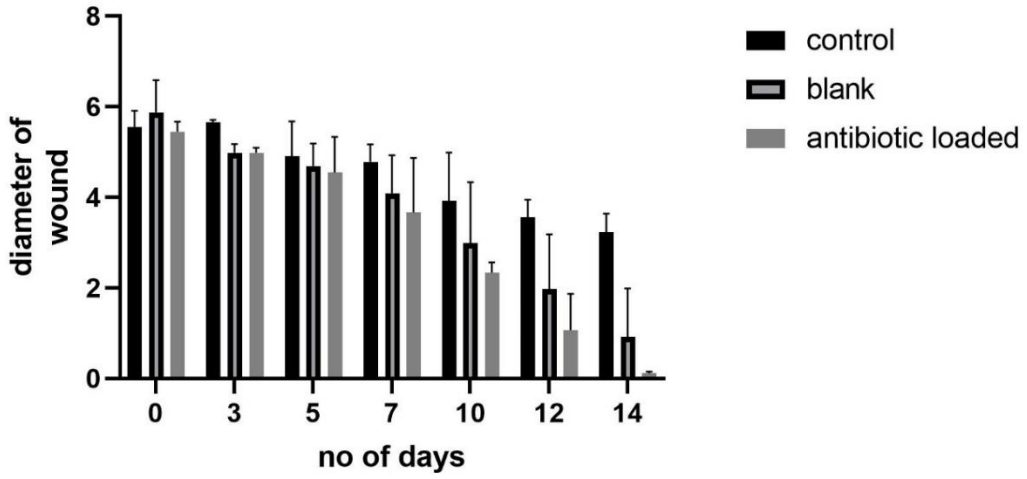

Figure 8. Wound healing activity.

Table 8. Effect of lincomycin NPs gel (2000mg/kg) on liver and kidney function test in acute toxicity study.

Parameters	Units	Control	Blank Treated	Lincomycin HCl treated
Bilirubin	mg/dL	0.20±0.01	0.33±0.017^{ns}	0.3±0.023
ALT	µ/L	48.0±1.65	76.0±2.43*	61±2.87
AST	µ/L	241±1.80	331±2.54^{ns}	272±2.64
Alkaline Phosphatase	µ/L	243±3.03	298±3.35^{ns}	341±3.84
Protein	g/dL	7.5±0.23	6.7±0.19^{ns}	6.9±0.25
Albumin	g/dL	4.3±0.15	3.7±0.09^{ns}	4.0±0.04
Globulin	g/dL	3.2±0.122	3.0±0.16^{ns}	2.9±0.21
Blood urea	mg/dL	53.0±1.41	49±1.65^{ns}	46±1.92
Serum creatinine	mg/dL	0.42±0.034	0.33±0.025^{ns}	0.31±0.043

The provided data from the table indicates that within the groups provided with treatment, there were observed elevations in blood urea levels accompanied by lower creatinine levels. Alkaline phosphatase, bilirubin, protein, albumin, and globulin levels were found to be within the normal range as observed in Table 8. However, there were elevated levels of AST (Aspartate Aminotransferase) and ALT (Alanine Aminotransferase) enzymes noted. This pattern suggests potential renal involvement, as evidenced by elevated blood urea levels coupled with lower creatinine levels, indicative of altered kidney function. Meanwhile, the normal range of alkaline phosphatase, bilirubin, protein, albumin, and globulin suggests intact liver and hepatic function. The elevation in AST and ALT enzymes indicates liver injury or damage, which could be associated with the treatment administered as it is determined in Figure 9.

 doi:10.20944/preprints202502.2311.v1

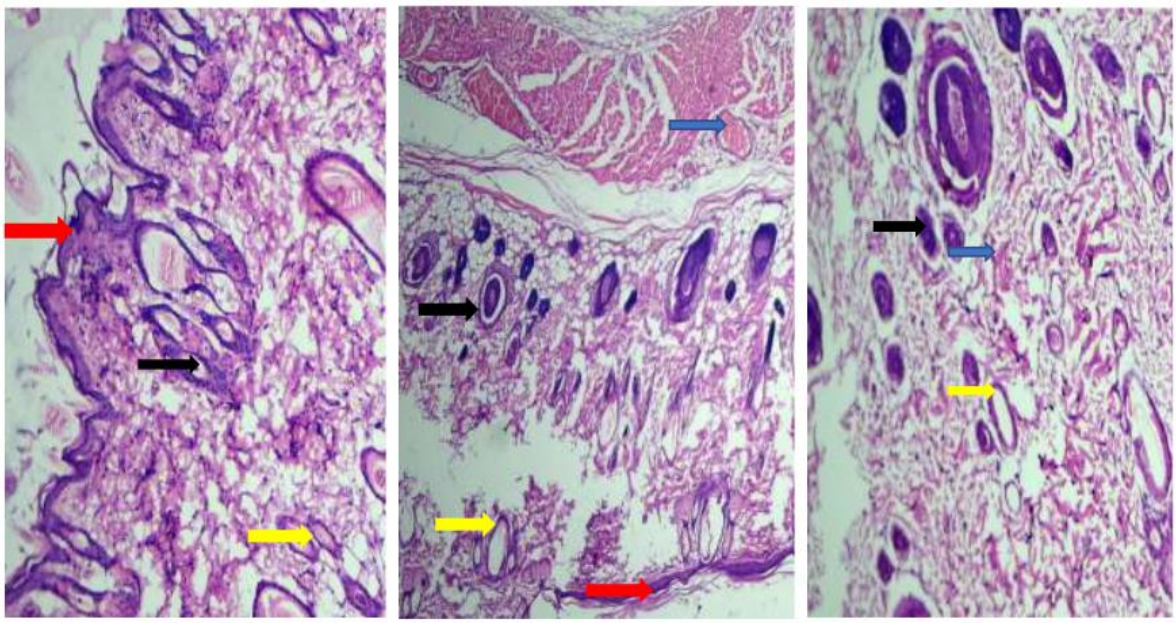

Figure 9. Histopathological studies a: G1(control), b: B1(blank), c: R1(loaded). Black: Macrophages, Yellow: Monocytes, Red: Epidermis, Blue: Erythrocytes.

4. Discussion

In pale skinned person rodents, wound mending viability was assessed utilizing a full-thickness excisional wound model. Different composite gels, including a clear gel and gels stacked with lincomycin HCl, were tried, with a benchmark group left untreated for examination. The level of twisted constriction for the advanced details was looked at against both the control and the clear gel, as displayed in Figure 9. On the third day, the stacked composite gel showed a tremendous impact on injury conclusion contrasted with the control and clear layers. This pattern of diminished injury size endured on the fifth and seventh days, with up to 76% compression noticed for the ideal definitions. All through the review span, all injuries slowly shut, accomplishing total conclusion by day 12 of treatment, as portrayed in Figure 9. The in-vivo concentrate on results recommend that the stacked plan assumed a vital part in improving cell movement and advancing early injury conclusion. These gainful impacts can be credited to the presence of lincomycin HCl in the composite gels, which forestalled contaminations, a vital figure postponed wound recuperating. Furthermore, the antimicrobial, cancer prevention agent, and calming properties of chitosan added to speeding up the mending system. Significantly, no cases of skin bothering responses were noticed all through the whole review period.

5. Conclusions

Our essential target of accomplishing broadened drug discharge abilities while keeping up with vigorous mechanical properties to endure organic difficulties is in arrangement with our definitive objective of guaranteeing successful antimicrobial adequacy. Lincomycin HCl nanoparticles have arisen as promising possibility for drug transporters in antimicrobial applications, especially in tending to antimicrobial obstruction. These nanoparticles offer the potential for both supported and controlled drug discharge in light of pH changes, giving a flexible answer for fighting microbial difficulties.

Informed Content Statement: Not applicable.

Funding: Not applicable.

Institution Review Board Statement: The analysis was led with the authorization of the Institutional Survey Board (IRB) at GC College, and the reference number GCUF/ERC/424.

 doi:10.20944/preprints202502.2311.v1

References

1. Abd-Allah, H., Abdel-Aziz, R. T., & Nasr, M. (2020). Chitosan nanoparticles making their way to clinical practice: A feasibility study on their topical use for acne treatment. International journal of biological macromolecules, 156, 262-270.
2. Ahmad, S., Zhu, X., Luo, J., Shen, M., Zhou, S., & Zhang, S. (2019). Conversion of phosphorus and nitrogen in lincomycin residue during microwave-assisted hydrothermal liquefaction and its application for Pb2+ removal. Science of the Total Environment, 687, 1381-1388.
3. Alqahtani, F. Y., Aleanizy, F. S., El Tahir, E., Alquadeib, B. T., Alsarra, I. A., Alanazi, J. S., & Abdelhady, H. G. (2019). Preparation, characterization, and antibacterial activity of diclofenac-loaded chitosan nanoparticles. Saudi Pharmaceutical Journal, 27(1), 82-87.
4. Anicuta, S.-G., Dobre, L., Stroescu, M., & Jipa, I. (2010). Fourier transform infrared (FTIR) spectroscopy for characterization of antimicrobial films containing chitosan. Analele Universită Ńii din Oradea Fascicula: Ecotoxicologie, Zootehnie şi Tehnologii de Industrie Alimentară, 2010, 1234-1240.
5. Banik, N., Hussain, A., Ramteke, A., Sharma, H. K., & Maji, T. K. (2012). Preparation and evaluation of the effect of particle size on the properties of chitosan-montmorillonite nanoparticles loaded with isoniazid. RSC advances, 2(28), 10519-10528.
6. Benamer Oudih, S., Tahtat, D., Nacer Khodja, A., Mahlous, M., Hammache, Y., Guittoum, A. E., & Kebbouche Gana, S. (2023). Chitosan nanoparticles with controlled size and zeta potential. Polymer Engineering & Science, 63(3), 1011-1021.
7. Chandrasekaran, M., Kim, K. D., & Chun, S. C. (2020). Antibacterial activity of chitosan nanoparticles: A review. Processes, 8(9), 1173.
8. Divya, K., Vijayan, S., George, T. K., & Jisha, M. (2017). Antimicrobial properties of chitosan nanoparticles: Mode of action and factors affecting activity. Fibers and polymers, 18, 221-230.
9. Dong, W., Ye, J., Wang, W., Yang, Y., Wang, H., Sun, T., . . . Liu, Y. (2020). Self-assembled lecithin/chitosan nanoparticles based on phospholipid complex: a feasible strategy to improve entrapment efficiency and transdermal delivery of the poorly lipophilic drug. International Journal of Nanomedicine, 5629-5643.
10. El-Hadedy, D., & El-Nour, S. A. (2012). Identification of Staphylococcus aureus and Escherichia coli isolated from Egyptian food by conventional and molecular methods. Journal of Genetic Engineering and Biotechnology, 10(1), 129-135.
11. Ganjoo, R., Soni, S., Ram, V., & Verma, A. (2016). Medium molecular weight chitosan as a carrier for delivery of lincomycin hydrochloride from intra-pocket dental film: Design, development, in vitro and ex vivo characterization. Journal of Applied Pharmaceutical Science, 6(10), 008-019.
12. Garg, U., Chauhan, S., Nagaich, U., & Jain, N. (2019). Current advances in chitosan nanoparticles based drug delivery and targeting. Advanced pharmaceutical bulletin, 9(2), 195.
13. Gokce, Y., Cengiz, B., Yildiz, N., Calimli, A., & Aktas, Z. (2014). Ultrasonication of chitosan nanoparticle suspension: Influence on particle size. Colloids and Surfaces A: Physicochemical and Engineering Aspects, 462, 75-81.
14. Hadidi, M., Pouramin, S., Adinepour, F., Haghani, S., & Jafari, S. M. (2020). Chitosan nanoparticles loaded with clove essential oil: Characterization, antioxidant and antibacterial activities. Carbohydrate Polymers, 236, 116075.
15. Hasan, T. H., & Al-Harmoosh, R. A. (2020). Mechanisms of antibiotics resistance in bacteria. Sys Rev Pharm, 11(6), 817-823.
16. Hassani, S., Laouini, A., Fessi, H., & Charcosset, C. (2015). Preparation of chitosan–TPP nanoparticles using microengineered membranes–Effect of parameters and encapsulation of tacrine. Colloids and Surfaces A: Physicochemical and Engineering Aspects, 482, 34-43.
17. He, G., Chen, X., Yin, Y., Cai, W., Ke, W., Kong, Y., & Zheng, H. (2016). Preparation and antibacterial properties of O-carboxymethyl chitosan/lincomycin hydrogels. Journal of Biomaterials Science, Polymer Edition, 27(4), 370-384.
18. Hejjaji, E. M., Smith, A. M., & Morris, G. A. (2018). Evaluation of the mucoadhesive properties of chitosan nanoparticles prepared using different chitosan to tripolyphosphate (CS: TPP) ratios. International journal of biological macromolecules, 120, 1610-1617.

 doi:10.20944/preprints202502.2311.v1

19. Hussain, Z., & Sahudin, S. (2016). Preparation, characterisation and colloidal stability of chitosan-tripolyphosphate nanoparticles: Optimisation of formulation and process parameters. Int J Pharm Pharm Sci, 8(3), 297-308.
20. Ibrahim, I. A., Ebeid, H. M., Kishk, Y. F., Abdel Fattah, A. F. A. K., Mahmoud, K. F., Ibrahim, A., . . . Mahmoud, K. (2019). Effect of grinding and particle size on some physical and rheological properties of chitosan. Arab Universities Journal of Agricultural Sciences, 27(2), 1513-1527.
21. Jiménez-Gómez, C. P., & Cecilia, J. A. (2020). Chitosan: a natural biopolymer with a wide and varied range of applications. Molecules, 25(17), 3981.
22. Jonassen, H., Kjøniksen, A.-L., & Hiorth, M. (2012). Effects of ionic strength on the size and compactness of chitosan nanoparticles. Colloid and Polymer Science, 290, 919-929.
23. Khan, E. A., Ma, J., Xiaobin, M., Jie, Y., Mengyue, L., Hong, L., . . . Liu, A. (2022). Safety evaluation study of lincomycin and spectinomycin hydrochloride intramuscular injection in chickens. Toxicology Reports, 9, 204-209.
24. Kshirsagar, N. (2000). Drug delivery systems. Indian Journal of Pharmacology, 32(4), 54-61.
25. Kumar, R., & Tyagi, C. (2022). PREPARATION AND EVALUATION OF LIPOSOMAL GEL OF LINCOMYCIN HCL.
26. Kumar, S., & Maurya, H. (2018). An Overview on Advance Vesicles Formulation as a Drug Carrier for NDDS. European Journal of Biomedical, 5(2), 292-303.
27. Levy, S. B., & Marshall, B. (2004). Antibacterial resistance worldwide: causes, challenges and responses. Nature medicine, 10(Suppl 12), S122-S129.
28. Leyva-Porras, C., Cruz-Alcantar, P., Espinosa-Solís, V., Martínez-Guerra, E., Piñón-Balderrama, C. I., Compean Martínez, I., & Saavedra-Leos, M. Z. (2019). Application of differential scanning calorimetry (DSC) and modulated differential scanning calorimetry (MDSC) in food and drug industries. Polymers (Basel), 12(1), 5.
29. Liu, J., Li, S., Wang, J., Li, N., Zhou, J., & Chen, H. (2023). Application of nano drug delivery system (NDDS) in cancer therapy: A perspective. Recent patents on anti-cancer drug discovery, 18(2), 125-132.
30. Marei, N. H., Abd El-Samie, E., Salah, T., Saad, G. R., & Elwahy, A. H. (2016). Isolation and characterization of chitosan from different local insects in Egypt. International journal of biological macromolecules, 82, 871-877.
31. Modi, S., & Anderson, B. D. (2013). Determination of drug release kinetics from nanoparticles: overcoming pitfalls of the dynamic dialysis method. Molecular pharmaceutics, 10(8), 3076-3089.
32. Murugaiyan, J., Kumar, P. A., Rao, G. S., Iskandar, K., Hawser, S., Hays, J. P., . . . Jose, R. A. M. (2022). Progress in alternative strategies to combat antimicrobial resistance: Focus on antibiotics. Antibiotics, 11(2), 200.
33. Najim, S. S. (2017). SPECTROPHTOMETERIC DETERMINATION OF LINCOMYCIN IN PHARMACEUTICAL MEDICATION.
34. Pan, C., Qian, J., Zhao, C., Yang, H., Zhao, X., & Guo, H. (2020). Study on the relationship between crosslinking degree and properties of TPP crosslinked chitosan nanoparticles. Carbohydrate Polymers, 241, 116349.
35. Papathoti, N. K. Pervaiz, F., Mushtaq, R., & Noreen, S. (2021). Formulation and optimization of terbinafine HCl loaded chitosan/xanthan gum nanoparticles containing gel: Ex-vivo permeation and in-vivo antifungal studies. Journal of Drug Delivery Science and Technology, 66, 102935.
36. Popescu-Pelin, G., Fufă, O., Popescu, R. C., Savu, D., Socol, M., Zgură, I., . . . Socol, G. (2018). Lincomycin–embedded PANI–based coatings for biomedical applications. Applied Surface Science, 455, 653-666. doi: https://doi.org/10.1016/j.apsusc.2018.06.016
37. Qi, L., Xu, Z., Jiang, X., Hu, C., & Zou, X. (2004). Preparation and antibacterial activity of chitosan nanoparticles. Carbohydrate research, 339(16), 2693-2700.
38. Qing, X., He, G., Liu, Z., Yin, Y., Cai, W., Fan, L., & Fardim, P. (2021). Preparation and properties of polyvinyl alcohol/N–succinyl chitosan/lincomycin composite antibacterial hydrogels for wound dressing. Carbohydrate Polymers, 261, 117875.

 doi:10.20944/preprints202502.2311.v1

39. Ruiz-Pulido, G., & Medina, D. I. (2021). An overview of gastrointestinal mucus rheology under different pH conditions and introduction to pH-dependent rheological interactions with PLGA and chitosan nanoparticles. European Journal of Pharmaceutics and Biopharmaceutics, 159, 123-136.
40. Saadatkhah, N., Carillo Garcia, A., Ackermann, S., Leclerc, P., Latifi, M., Samih, S., . . . Chaouki, J. (2020). Experimental methods in chemical engineering: Thermogravimetric analysis—TGA. The Canadian Journal of Chemical Engineering, 98(1), 34-43.
41. Safari, J., & Zarnegar, Z. (2014). Advanced drug delivery systems: Nanotechnology of health design A review. Journal of Saudi Chemical Society, 18(2), 85-99.
42. Saraiva, S. M., Crespo, A. M., Vaz, F., Filipe, M., Santos, D., Jacinto, T. A., . . . Coutinho, P. (2023). Development and Characterization of Thermal Water Gel Comprising Helichrysum italicum Essential Oil-Loaded Chitosan Nanoparticles for Skin Care. Cosmetics, 10(1), 8.
43. Sethi, A., Ahmad, M., Huma, T., Khalid, I., & Ahmad, I. (2021). Evaluation of low molecular weight cross linked chitosan nanoparticles, to enhance the bioavailability of 5-flourouracil. Dose-Response, 19(2), 15593258211025353.
44. Sharma, M. (2019). Transdermal and intravenous nano drug delivery systems: present and future Applications of targeted nano drugs and delivery systems (pp. 499-550): Elsevier.
45. Shirolkar, M. M., Athavale, R., Ravindran, S., Rale, V., Kulkarni, A., & Deokar, R. (2021). Antibiotics functionalization intervened morphological, chemical and electronic modifications in chitosan nanoparticles. Nano-Structures & Nano-Objects, 25, 100657.
46. Singh Malik, D., Mital, N., & Kaur, G. (2016). Topical drug delivery systems: a patent review. Expert opinion on therapeutic patents, 26(2), 213-228.
47. Sobhani, Z., Samani, S. M., Montaseri, H., & Khezri, E. (2017). Nanoparticles of chitosan loaded ciprofloxacin: fabrication and antimicrobial activity. Advanced pharmaceutical bulletin, 7(3), 427.
48. Tantala, J., Thumanu, K., & Rachtanapun, C. (2019). An assessment of antibacterial mode of action of chitosan on Listeria innocua cells using real-time HATR-FTIR spectroscopy. International journal of biological macromolecules, 135, 386-393.
49. Thandapani, G., Prasad, S., Sudha, P., & Sukumaran, A. (2017). Size optimization and in vitro biocom46. patibility studies of chitosan nanoparticles. International journal of biological macromolecules, 104, 1794-1806.
50. Tiwari, G., Tiwari, R., Sriwastawa, B., Bhati, L., Pandey, S., Pandey, P., & Bannerjee, S. K. (2012). Drug delivery systems: An updated review. International journal of pharmaceutical investigation, 2(1), 2.
51. Weng, J., Tong, H. H., & Chow, S. F. (2020). In vitro release study of the polymeric drug nanoparticles: development and validation of a novel method. Pharmaceutics, 12(8), 7
52. Abd-Allah, H., Abdel-Aziz, R. T., & Nasr, M. (2020). Chitosan nanoparticles making their way to clinical practice: A feasibility study on their topical use for acne treatment. *International journal of biological macromolecules, 156*, 262-270.
53. Agarwal, M., Agarwal, M. K., Shrivastav, N., Pandey, S., Das, R., & Gaur, P. (2018). Preparation of chitosan nanoparticles and their in-vitro characterization. *International Journal of Life-Sciences Scientific Research, 4*(2), 1713-1720.
54. Ahmad, S., Zhu, X., Luo, J., Shen, M., Zhou, S., & Zhang, S. (2019). Conversion of phosphorus and nitrogen in lincomycin residue during microwave-assisted hydrothermal liquefaction and its application for Pb2+ removal. *Science of the Total Environment, 687*, 1381-1388.
55. Ahmet, U. (2020). Preparation of allantoin loaded chitosan nanoparticles and influence of molecular weight of chitosan on drug release. *İnönü Üniversitesi Sağlık Hizmetleri Meslek Yüksek Okulu Dergisi, 8*(3), 725-740.
56. Algharib, S. A., Dawood, A., Zhou, K., Chen, D., Li, C., Meng, K., . . . Huang, L. (2022). Preparation of chitosan nanoparticles by ionotropic gelation technique: Effects of formulation parameters and in vitro characterization. *Journal of Molecular Structure, 1252*, 132129.
57. Alqahtani, F. Y., Aleanizy, F. S., El Tahir, E., Alquadeib, B. T., Alsarra, I. A., Alanazi, J. S., & Abdelhady, H. G. (2019). Preparation, characterization, and antibacterial activity of diclofenac-loaded chitosan nanoparticles. *Saudi pharmaceutical journal, 27*(1), 82-87.

 doi:10.20944/preprints202502.2311.v1

58. Alqahtani, M. S., Al-Yousef, H. M., Alqahtani, A. S., Rehman, M. T., AlAjmi, M. F., Almarfidi, O., . . . Syed, R. (2021). Preparation, characterization, and in vitro-in silico biological activities of Jatropha pelargoniifolia extract loaded chitosan nanoparticles. *International Journal of Pharmaceutics, 606*, 120867.
59. Athavale, R., Sapre, N., Rale, V., Tongaonkar, S., Manna, G., Kulkarni, A., & Shirolkar, M. M. (2022). Tuning the surface charge properties of chitosan nanoparticles. *Materials Letters, 308*, 131114.
60. Basha, M., AbouSamra, M. M., Awad, G. A., & Mansy, S. S. (2018). A potential antibacterial wound dressing of cefadroxil chitosan nanoparticles in situ gel: Fabrication, in vitro optimization and in vivo evaluation. *International Journal of Pharmaceutics, 544*(1), 129-140.
61. Bin-Jumah, M., Gilani, S. J., Jahangir, M. A., Zafar, A., Alshehri, S., Yasir, M., . . . Imam, S. S. (2020). Clarithromycin-loaded ocular chitosan nanoparticle: formulation, optimization, characterization, ocular irritation, and antimicrobial activity. *International Journal of Nanomedicine*, 7861-7875.
62. Chandrasekaran, M., Kim, K. D., & Chun, S. C. (2020). Antibacterial activity of chitosan nanoparticles: A review. *Processes, 8*(9), 1173.
63. Cheah, Y. J., Yunus, M. H. M., Fauzi, M. B., Tabata, Y., Hiraoka, Y., Phang, S. J., . . . Yazid, M. D. (2023). Gelatin–chitosan–cellulose nanocrystals as an acellular scaffold for wound healing application: fabrication, characterisation and cytocompatibility towards primary human skin cells. *Cellulose, 30*(8), 5071-5092.
64. Chhibber, T., Gondil, V. S., & Sinha, V. (2020). Development of chitosan-based hydrogel containing antibiofilm agents for the treatment of Staphylococcus aureus–infected burn wound in mice. *Aaps Pharmscitech, 21*, 1-12.
65. Divya, K., & Jisha, M. (2018). Chitosan nanoparticles preparation and applications. *Environmental chemistry letters, 16*, 101-112.
66. Divya, K., Vijayan, S., George, T. K., & Jisha, M. (2017). Antimicrobial properties of chitosan nanoparticles: Mode of action and factors affecting activity. *Fibers and polymers, 18*, 221-230.
67. Fatima, M., Sheikh, A., Abourehab, M. A., & Kesharwani, P. (2022). Advancements in polymeric nanocarriers to mediate targeted therapy against triple-negative breast cancer. *Pharmaceutics, 14*(11), 2432.
68. Grumezescu, V., Negut, I., Gherasim, O., Birca, A. C., Grumezescu, A. M., Hudita, A., . . . Holban, A. M. (2019). Antimicrobial applications of MAPLE processed coatings based on PLGA and lincomycin functionalized magnetite nanoparticles. *Applied Surface Science, 484*, 587-599.
69. Gurses, M. S., Erkey, C., Kizilel, S., & Uzun, A. (2018). Characterization of sodium tripolyphosphate and sodium citrate dehydrate residues on surfaces. *Talanta, 176*, 8-16.
70. Hejjaji, E. M., Smith, A. M., & Morris, G. A. (2018). Evaluation of the mucoadhesive properties of chitosan nanoparticles prepared using different chitosan to tripolyphosphate (CS: TPP) ratios. *International journal of biological macromolecules, 120*, 1610-1617.
71. Jain, K. K. (2008). *Drug delivery systems* (Vol. 251): Springer.
72. Khalil, R. M., El Arini, S. K., AbouSamra, M. M., Zaki, H. S., El-Gazaerly, O. N., & Elbary, A. A. (2021). Development of lecithin/chitosan nanoparticles for promoting topical delivery of propranolol hydrochloride: Design, optimization and in-vivo evaluation. *Journal of pharmaceutical sciences, 110*(3), 1337-1348.
73. Khan, F., Yu, H., & Kim, Y.-M. (2020). Bactericidal activity of usnic acid-chitosan nanoparticles against persister cells of biofilm-forming pathogenic bacteria. *Marine Drugs, 18*(5), 270.
74. Liu, D., Yang, F., Xiong, F., & Gu, N. (2016). The smart drug delivery system and its clinical potential. *Theranostics, 6*(9), 1306.
75. Mandal, A. S., Biswas, N., Karim, K. M., Guha, A., Chatterjee, S., Behera, M., & Kuotsu, K. (2010). Drug delivery system based on chronobiology—A review. *Journal of controlled release, 147*(3), 314-325.
76. Marei, N. H., Abd El-Samie, E., Salah, T., Saad, G. R., & Elwahy, A. H. (2016). Isolation and characterization of chitosan from different local insects in Egypt. *International journal of biological macromolecules, 82*, 871-877.
77. Mu, W., Chu, Q., Liu, Y., & Zhang, N. (2020). A review on nano-based drug delivery system for cancer chemoimmunotherapy. *Nano-micro letters, 12*, 1-24.
78. Najim, S. S. (2017). SPECTROPHTOMETERIC DETERMINATION OF LINCOMYCIN IN PHARMACEUTICAL MEDICATION.

 doi:10.20944/preprints202502.2311.v1

79. Nguyen, T. V., Nguyen, T. T. H., Wang, S.-L., Vo, T. P. K., & Nguyen, A. D. (2017). Preparation of chitosan nanoparticles by TPP ionic gelation combined with spray drying, and the antibacterial activity of chitosan nanoparticles and a chitosan nanoparticle–amoxicillin complex. *Research on Chemical Intermediates, 43*, 3527-3537.
80. Noreen, S., Pervaiz, F., Ashames, A., Buabeid, M., Fahelelbom, K., Shoukat, H., . . . Murtaza, G. (2021). Optimization of novel naproxen-loaded chitosan/carrageenan nanocarrier-based gel for topical delivery: Ex vivo, histopathological, and in vivo evaluation. *Pharmaceuticals, 14*(6), 557.
81. Pan, C., Qian, J., Zhao, C., Yang, H., Zhao, X., & Guo, H. (2020). Study on the relationship between crosslinking degree and properties of TPP crosslinked chitosan nanoparticles. *Carbohydrate Polymers, 241*, 116349.
82. Pawar, H. V., Tetteh, J., Debrah, P., & Boateng, J. S. (2019). Comparison of in vitro antibacterial activity of streptomycin-diclofenac loaded composite biomaterial dressings with commercial silver based antimicrobial wound dressings. *International journal of biological macromolecules, 121*, 191-199.
83. Pervaiz, F., Mushtaq, R., & Noreen, S. (2021). Formulation and optimization of terbinafine HCl loaded chitosan/xanthan gum nanoparticles containing gel: Ex-vivo permeation and in-vivo antifungal studies. *Journal of Drug Delivery Science and Technology, 66*, 102935.
84. Popescu-Pelin, G., Fufă, O., Popescu, R., Savu, D., Socol, M., Zgură, I., . . . Socol, G. (2018). Lincomycin–embedded PANI–based coatings for biomedical applications. *Applied Surface Science, 455*, 653-666.
85. Qing, X., He, G., Liu, Z., Yin, Y., Cai, W., Fan, L., & Fardim, P. (2021). Preparation and properties of polyvinyl alcohol/N–succinyl chitosan/lincomycin composite antibacterial hydrogels for wound dressing. *Carbohydrate Polymers, 261*, 117875.
86. Rajendran, N. K., Kumar, S. S. D., Houreld, N. N., & Abrahamse, H. (2018). A review on nanoparticle based treatment for wound healing. *Journal of Drug Delivery Science and Technology, 44*, 421-430.
87. Roy, H., Nayak, B. S., Maddiboyina, B., & Nandi, S. (2022). Chitosan based urapidil microparticle development in approach to improve mechanical strength by cold hyperosmotic dextrose solution technique. *Journal of Drug Delivery Science and Technology, 76*, 103745.
88. Saraiva, S. M., Crespo, A. M., Vaz, F., Filipe, M., Santos, D., Jacinto, T. A., . . . Coutinho, P. (2023). Development and Characterization of Thermal Water Gel Comprising Helichrysum italicum Essential Oil-Loaded Chitosan Nanoparticles for Skin Care. *Cosmetics, 10*(1), 8.
89. Sethi, A., Ahmad, M., Huma, T., Khalid, I., & Ahmad, I. (2021). Evaluation of low molecular weight cross linked chitosan nanoparticles, to enhance the bioavailability of 5-flourouracil. *Dose-Response, 19*(2), 15593258211025353.
90. Shantier, S. W., Elimam, M. M., Mohamed, M. A., & Gadkariem, E. A. (2017). Stability studies on lincomycin HCl using validated developed second derivative spectrophotometric method. *J Innov Pharm Biol Sci, 4*(4), 141-144.
91. Skwarczynski, M., Bashiri, S., Yuan, Y., Ziora, Z. M., Nabil, O., Masuda, K., . . . Ruktanonchai, U. (2022). Antimicrobial activity enhancers: towards smart delivery of antimicrobial agents. *Antibiotics, 11*(3), 412.
92. Sobhani, Z., Samani, S. M., Montaseri, H., & Khezri, E. (2017). Nanoparticles of chitosan loaded ciprofloxacin: fabrication and antimicrobial activity. *Advanced pharmaceutical bulletin, 7*(3), 427.
93. Vikas, K., Arvind, S., Ashish, S., Gourav, J., & Vipasha, D. (2011). Recent advances in ndds (novel drug delivery system) for delivery of anti-hypertensive drugs. *Int J Drug Dev Res, 3*(1), 252-259.
94. Wang, W., Meng, Q., Li, Q., Liu, J., Zhou, M., Jin, Z., & Zhao, K. (2020). Chitosan derivatives and their application in biomedicine. *International Journal of Molecular Sciences, 21*(2), 487.
95. Yao, J., Yang, B., Chen, K., Sun, H., Zhu, Z., Yin, W., . . . Sheng, Q. (2021). Sodium tripolyphosphate as a selective depressant for separating magnesite from dolomite and its depression mechanism. *Powder Technology, 382*, 244-253.
96. Yassin, A. E., Albekairy, A. M., Omer, M. E., Almutairi, A., Alotaibi, Y., Althuwaini, S., . . . Alluhaim, W. (2023). Chitosan-Coated Azithromycin/Ciprofloxacin-Loaded Polycaprolactone Nanoparticles: A Characterization and Potency Study. *Nanotechnology, Science and Applications*, 59-72.

 doi:10.20944/preprints202502.2311.v1